Open Access

Advances in Environmental and Engineering Research

LIDSEN Publishing Inc.

Original Research

Poly (Lactic Acid) (PLA)/Recycled Styrene Butadiene Rubber (rSBR) Composites

Étienne Cusson [1, †], Jean-Christophe Mougeot [2, †], Mélanie Maho [2, †], Florian Lacroix [2, †], Ali Fazli [1, †], Denis Rodrigue [1, †, *]

1. Department of Chemical Engineering, Université Laval, Quebec, QC, Canada; E-Mails: etienne.cusson.1@ulaval.ca; ali.fazli.1@ulaval.ca; Denis.Rodrigue@gch.ulaval.ca
2. Laboratoire de Mécanique Gabriel Lamé, Université de Tours, INSA CVL, Université d'Orléans, 29 rue des Martyrs, 37300, Joué les Tours, France; E-Mails: jean-christophe.mougeot@etu.univ-tours.fr; melanie.maho@etu.univ-tours.fr; f.lacroix@univ-tours.fr

† These authors contributed equally to this work.

* **Correspondence:** Denis Rodrigue; E-Mail: Denis.Rodrigue@gch.ulaval.ca

Academic Editor: Zed Rengel

Adv Environ Eng Res
2022, volume 3, issue 2
doi:10.21926/aeer.2202012

Received: March 01, 2022
Accepted: March 29, 2022
Published: April 11, 2022

Abstract

Recycled styrene butadiene rubber (rSBR) from waste car tires was used as a filler in poly(lactic) acid (PLA) to modify its properties. The compounds were prepared via twin-screw extrusion and molded by injection with different rSBR contents (0 to 25% wt.). Additionally, recycled rubber particle size was controlled between 125 and 1000 µm to determine the effect of this parameter. From the samples produced, a series of morphological, physical and mechanical characterizations were performed. As expected, rSBR addition decreased the PLA stiffness. Up to 5% rSBR, the flexural and elastic moduli were unchanged, but the tensile strength, elongation at break and impact toughness were decreased. The highest tensile strength, elongation at break and impact toughness were achieved for PLA/rSBR blends filled with small rubber particles (125-250 µm). According to the morphological analysis, this behavior was associated to better interfacial interactions between smaller rSBR particles (higher specific surface area) and PLA resulting in a more uniform filler distribution and better

stress transfer from PLA to rSBR. Finally, to complete the mechanical properties of the materials, fatigue tests were carried out on different blends and the results were related to instrumented indentation to get some more local information.

Keywords
Polylactic acid; styrene butadiene rubber; recycling; mechanical properties

1. Introduction

Recycled styrene butadiene rubber (rSBR), also known as waste rubber powder (WRP) or ground tire rubber (GTR), is a widely available synthetic rubber as virgin SBR is the most used rubber in car tires. Globally, with over a billion vehicles on the road, and with a limited life expectancy for tires, rSBR availability is expected to increase in the future [1]. For example, between 2 and 4 billion used tires are stacked in landfills in the United States alone [2]. Thus, the recovery of waste rubber is not only important for environmental issues, but is also an economically efficient way to manage the problem of scrap tire disposal [3]. To this end, different techniques (wet, ambient or cryogenic grinding) can be used to downsize the waste tires into more or less fine particles for easier processing. A review on current methods and applications can be found in Fazli and Rodrigue [4, 5].

During the last two decades, increasing environmental consciousness has driven both the scientific community and the chemical industry to find new applications for recycled materials. On the other hand, there is also an increased demand for biosourced and biodegradable polymers [6]. One of the main commercial materials leading this movement is polylactic acid (PLA) [7-10]. Being sourced from extensively available crops (such as corn and sugar beets), this thermoplastic resin offers a sustainable alternative to petroleum based polymers [7]. However, PLA still represents only a small fraction of the global demand for plastics. The main limitations for PLA are its high brittleness, poor impact resistance, and relatively high cost [8-11]. For this reason, there is a great deal of research done to develop and modify PLA blends for different applications. Using virgin elastomers (co-polymers) offers satisfactory results, but the costs of such blends is still too high for commercial productions [9, 10]. Recently, research using waste rubber as a filler in PLA blends has shown promising results [10]. Under specific conditions, impact toughness and elongation at break of PLA can be increased. For example, Yang et al. [12] showed that using recycled tire rubber for impact modification of PLA (14.47 kJ/m^2) generated significant improvement of impact strength (about 160%) of the resulting blends which was similar to the excellent toughening effect of styrene-butadiene-styrene block copolymer (SBS) (161.9% improvement) and higher than virgin ethylene-α-octene copolymer (EOC) (29.6%) and glycidyl methacrylate grafted EOC (mEOC) (52.4%). However, no information on the effect of rubber particle size on such blends was reported. In polymer blends, particle sizes are known to play a significant role in controlling the total contact surface area between the dispersed phase and the matrix [13, 14].

Fatigue studies are not systematically performed on thermoplastics and polymer blends/composites/foams. Nevertheless, they are highly performed on rubbers/elastomers, but face some limitations such as self-heating, large strains imposed, etc. [15, 16]. Furthermore, this type of approach is time, energy and material consuming. Although some publications can be found

on the fatigue behavior of SBR [17, 18], very limited information can be found on PLA alone (mainly from additive manufacturing) [19, 20] and even less on PLA/SBR blends. In general, it can be concluded that fatigue studies on compounds based on thermoplastic matrices and elastomer as fillers are not available, not to mention compounds made from recycled materials.

As far as instrumented indentation is concerned, the technique was mainly developed for metals. However, this is no longer the case as numerous applications can now be found from industrial to medical applications and more fundamental research. Different behaviours and structures are reported from very hard to very soft materials including elastic, plastic and/or viscoelastic behaviours for applications like adhesives, coatings, composites, biological tissues, etc. However, instrumented indentation is still poorly studied and development are still needed to adapt the theories for other materials (non-metallic) [21, 22]. This aspect is investigated in this work.

This study presents an investigation dedicated to the preparation and characterization of blends combining a biobased resin (PLA) with a recycled additive (rSBR) to produce more sustainable and inexpensive compounds. In particular, the effect of recycled fillers content and particle size on the blends properties prepared using standard melt processing in terms of phase morphology and mechanical properties are investigated with a focus on toughness and impact strength of PLA/rSBR since PLA alone is a very brittle bioplastic. To complete the mechanical behavior analysis of these blends, a campaign of fatigue tests and instrumented indentation tests were also carried out.

2. Experimental

2.1 Materials

The rSBR was supplied by *Recyc RPM* (Québec, Canada) in a powder form. The rSBR was initially obtained through mechanical recycling of waste tires. The material was then mechanically sieved to produce different particle sizes with four mesh openings (125, 250, 500 and 1000 µm) representing the classification of the particles diameter. Screening thus produced three distinct particle size ranges: 125-250 µm, 250-500 µm and 500-1000 µm are referred as SBR1, SBR2 and SBR3, respectively. Also, fourth particle size range was used based on the unsieved rSBR (SBRm) to determine the effects of a wider distribution range of particle sizes. The granulometric study of the rSBR (as received) revealed that 19% is between 125 to 250 µm, 66% is between 250 to 500 µm and 12% is between 500 to 1000 µm with traces of smaller and larger particles (less than 3%). The matrix used in this study was PLA grade 2003D produced by *NatureWorks LLC* (Minnesota, USA). It has a density of 1240 kg/m^3 and a melt flow index of 6 g/10 min (2.16 kg and 210 °C).

2.2 Production of PLA/rSBR Blends

Four different rSBR weight contents were used (5, 10, 15 and 25% wt.) for compounding via melt mixing of the rubber particle with PLA (matrix). The PLA (pellets) and rSBR (powders) were melt-blended via twin-screw extrusion. Both materials were fed separately and the feeding rates of each material was set according to the final concentration desired. A Leistritz ZSE-27 (D = 27 mm, L/D = 40) co-rotating twin-screw extruder composed of 10 heating zones was used. The rSBR and PLA were fed at the main feeder position (1st zone) and side-stuffer (4th zone) respectively, as determined in a previous study [13]. The temperature profile was set as 140, 160, 180, 180, 185, 185, 185, 180, 175 and 170 °C for the ten zones of the extruder with a die diameter of 3 mm. The

compounds were cooled down using a water bath before being air dried and fed to a pelletizer. The material was dried overnight in a convection oven at 55 °C before being injection molded on a Nissei model PS60E9ASE with an injection temperature of 180 °C and a mold temperature of 30 °C. The mold had the required dimensions for each characterization as described next.

2.3 Characterization

Micrographs were taken with a JEOL JSM-840A (Tokyo, Japan) scanning electron microscope (SEM). The samples were cryogenically fractured after being frozen in liquid nitrogen to expose their cross-section and coated with a thin layer of Au/Pd by a sputtering technique. Images were taken at different magnifications (15 kV).

Density was obtained using an ULTRAPYC 1200e gas (nitrogen) pycnometer. All the results are the average of at least three replicates.

Hardness was measured following ASTM D2240-15 [23] using a 307L model durometer (PTC Instruments, Los Angeles, USA). Due to the dual nature of the samples (blend of hard thermoplastic and soft elastic rubber), two scales (Shore A and Shore D) were used for each sample. All the results are the average of at least ten replicates.

Tensile tests were carried out at room temperature on an Instron (Norwood, USA) model 5565 universal testing machine (500 N load cell). The crosshead speed was set at 10 mm/min following ASTM D638-14 [24] to get the elastic modulus, tensile strength and elongation at break. The samples were type IV with a gauge length of 33 mm and 3.25 mm in thickness. All the results are the average of at least five measurements.

Flexural tests were done at room temperature using the same testing machine as for tensile tests (Instron 5565, Norwood, USA). The crosshead speed was set at 2 mm/min following ASTM D790-10 [25] to get the flexural modulus. The dimensions were 12.35 mm in width and 3.25 mm in thickness for a span length of 60 mm. All the results are the average of at least five repetitions.

Charpy impact tests were performed on a Tinius Olsen (Horsham, USA) model Impact 104 pendulum impact tester. According to ASTM D256-10 [26], the impact toughness was calculated by dividing the energy at break by the cross-sectional area of the sample. The samples had a 2 mm deep notch (ASM, Dynisco) with dimensions of 120 mm in length, 12 mm in width and 3.25 mm in thickness. All the results are the average of at least ten samples.

A tension-tension (T/T) fatigue test campaign was achieved on an Instron 8872 (Norwood, USA) 25 kN servo-hydraulic fatigue testing device. The frequency of the tests was set to 5 Hz and performed under controlled force. All the fatigue tests were done using a load ratio (*R*) of 1 defined as:

$$R = \frac{F_{min}}{F_{max}} \quad (1)$$

where F_{min} and F_{max} are the minimal and maximal force applied to the sample during a cycle. The dimensions are the same as those used for static tensile tests. Special attention was paid to the experimental conditions to avoid as much as possible the influence of the environment on the measurements. The sample was surrounded by a black cardboard box to limit any reflections and a dark sheet covered the experimental set-up.

To get more precise information on the local properties and especially on the rSBR dispersion, an instrumented indenter was used to achieve local mechanical characterization. These tests were performed on a NanoTest Micro-Materials Ldt allowing to apply forces up to 500 mN and coupled with a diamond Berkovich tip. A load-control method was used following a trapezoidal load history: loading (10 s), dwelling (hold at maximum load = 30 s) and unloading (10 s). These conditions were determined based on preliminary studies to avoid the effects of viscosity and provide an elastic response as much as possible. For the indentation dimensions, particular care was taken to obtain the lowest possible surface roughness on the samples and thus limit the dispersion in the results obtained. A typical profile consists in a matrix pattern of 25 indentations (5 × 5) in areas sufficiently far apart to obtain a representative result of the local mechanical behaviour. In total, 100 indentations were carried out for each sample. Each indentation was performed at 100 µm from the previous one to limit interactions, which is well above the recommendations available in the literature [27]. Then, the indentation curve was analyzed using the Oliver and Pharr method [28]. Based on this method and ISO 14577, the unloading curves were fitted from 100% to 20% of the maximum force (P_{max}). Then, the upper part of the unloading curve can be mathematically described by a power-law function as:

$$P = A\left(h - h_f\right)^m \tag{2}$$

where P is the force and h is the displacement. A and m are two material constants, while h_f is the final depth after complete unloading estimated by a least-square method.

Calculating the derivative of equation (2) leads to the slope of the unloading curve ($S = dP/dh$) evaluated at $P = P_{max}$ and $h = h_{max}$ to get:

$$S = Am\left(h_{max} - h_f\right)^{m-1} \tag{3}$$

It is then possible to obtain the contact depth h_c between the sample and the tip as:

$$h_c = h_{max} - \epsilon\frac{P_{max}}{S} \tag{4}$$

with P_{max} and h_{max} the maximal force and displacement respectively, while ϵ is a correction factor equal to 0.75 for a Berkovich tip [29].

At this given depth, the projected contact area A_p between the indentation tip and the sample is:

$$A_p = 24.5h_c^2 \tag{5}$$

It has been decided to use this perfect projected contact area for the used indentation depths since the apex default can be considered as negligible. Finally, the indentation modulus (E_r) was calculated from the Oliver and Pharr model as [28]:

$$E_r = \frac{s\sqrt{\pi}}{2\beta\sqrt{A_P}} \tag{6}$$

where β is a correction coefficient taking into account the axisymmetry of the indentor. The commonly used value for a Berkovich indentor is 1.034 [30].

3. Results and Discussion

3.1 Morphology

As shown in Figure 1, SEM micrographs reveals that blends containing SBR1 (smallest particle size) shows a somewhat well embedded rSBR particles inside the PLA matrix. Figure 1 shows that the interface between SBR1 and PLA is barely visible and detection of the rubber phase is difficult. As expected, addition of SBR1 (125-250 µm) with higher specific surface area compared to larger rSBR particles might show better interaction of embedded rubber particles (SBR1) with the matrix resulting in a more textured surface and uniform filler distribution [31]. It should be noticed that the processing conditions (shear/elongational stresses) can also be responsible for rSBR particle break-up for all particle sizes due to the mechanical energy imparted inside both processing equipment (extrusion and injection) [13, 32].

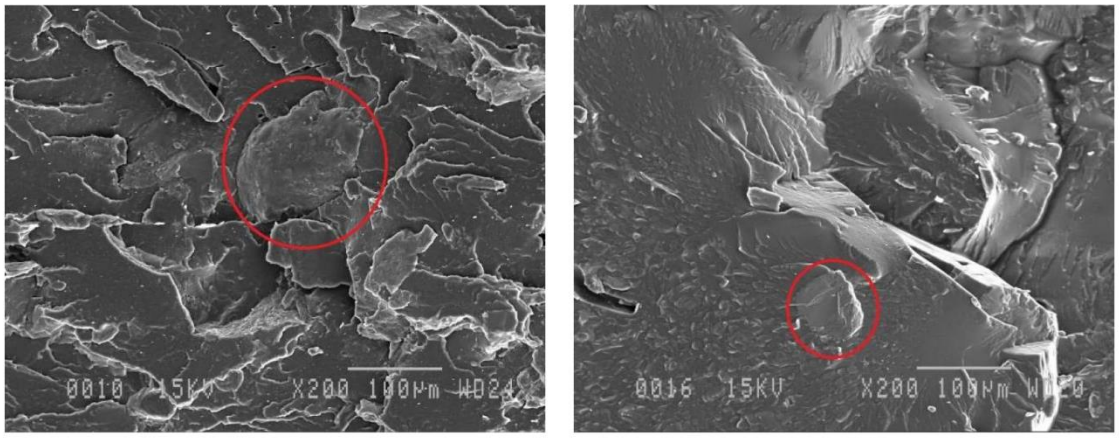

(**a**) (**b**)

Figure 1 SEM images of: a) PLA/SBR1 (5%) and b) PLA/SBR1 (25%). The circles indicate the position of a rSBR particle.

For blends using SBR2, the PLA/rSBR interface appears to be well bounded, although some voids can be seen at the interface and the SBR2 particles appear less spherical than SBR1 particles (125-250 µm). As shown in Figure 2, poor dispersion of SBR2 particles (250-500 µm) with low affinity towards the matrix may lead to the formation of voids around particles indicating high interfacial tension between PLA and rSBR (especially at 25% filler). Figure 2a shows that smaller particles can also be detected in the blend structure. This can be related to the processing conditions used as particle break-up can take place due to the mechanical energy imparted inside both processing equipment (extrusion and injection) [13]. Particle break-up and agglomeration (contact) can also be related to the rSBR concentration selected and therefore the rSBR contents were limited to 25% wt. (negligible particle-particle interactions if good distribution is produced).

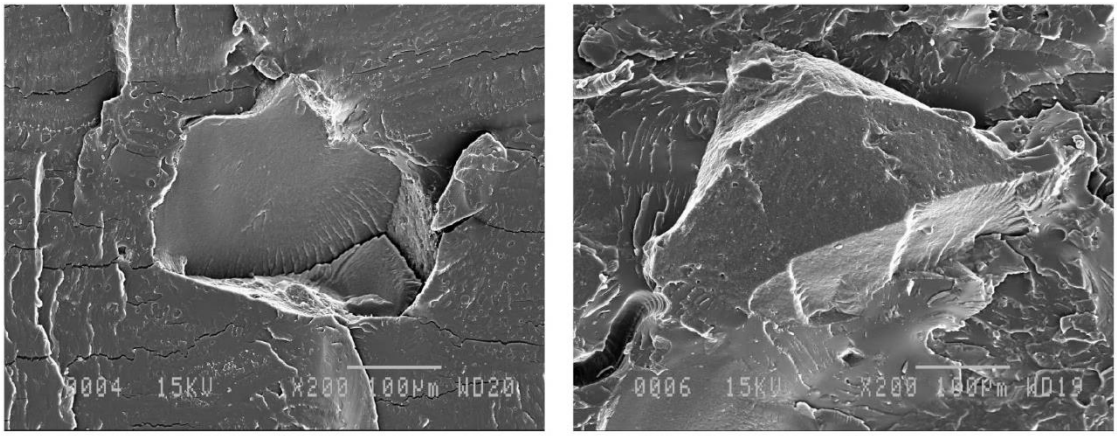

Figure 2 SEM images of: a) PLA/SBR2 (5%) and b) PLA/SBR2 (25%).

For samples prepared with SBR3, the interface quality was found to be highly variable from one particle to another. Sometimes the rSBR particles appear to be well embedded like in Figure 3a, while in other cases they are clearly sticking out of the fracture plane (Figure 3b). Again, SBR3 particles are much less spherical than for SBR1. As shown in SEM images (Figures 1-3), poorly bonded rSBR to the PLA matrix led to clean and smooth surface indicating some incompatibility and low affinity between the rSBR (crosslinked recycled rubber) and PLA, especially with increasing rSBR content from 5 to 25%.

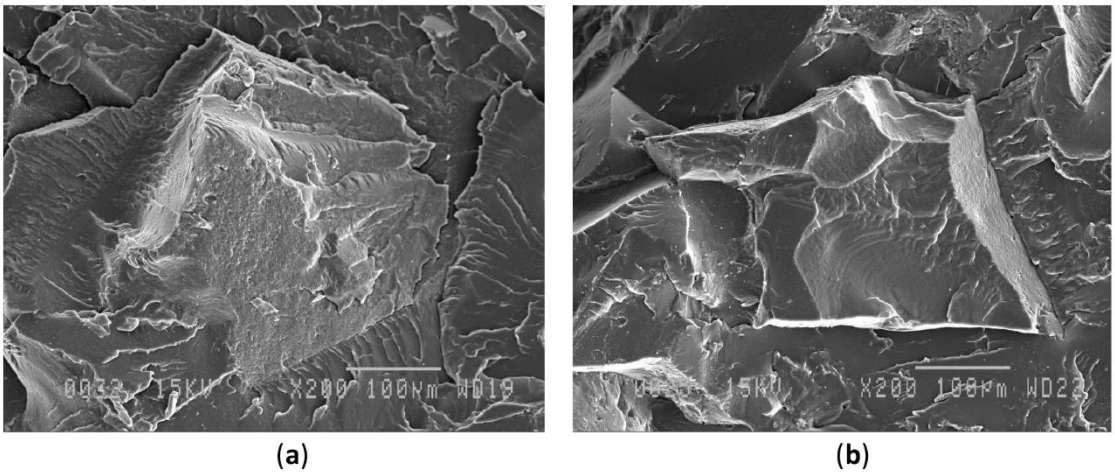

Figure 3 SEM images of: a) PLA/SBR3 (5%) and b) PLA/SBR3 (25%).

Finally, Figure 4 presents a typical morphology for samples prepared using a wide particle size distribution (SBRm). Small particles are clearly seen (<125 µm) which might also come from the initial material and break-up while processing. But microcracks are also seen originating from the rSBR particle surface, especially from larger particles. This observation can lead to two important conclusions. Firstly, larger particles are more detrimental for the mechanical performance of the compounds. Secondly, even if good particle-matrix contact can be achieved, there is probably poor interfacial adhesion/interaction due to the crosslink nature of the rSBR particles (limited surface chain mobility) and the different chemical nature of both components (rSBR vs. PLA). In both cases, improvements are possible but not included in this work as a first step.

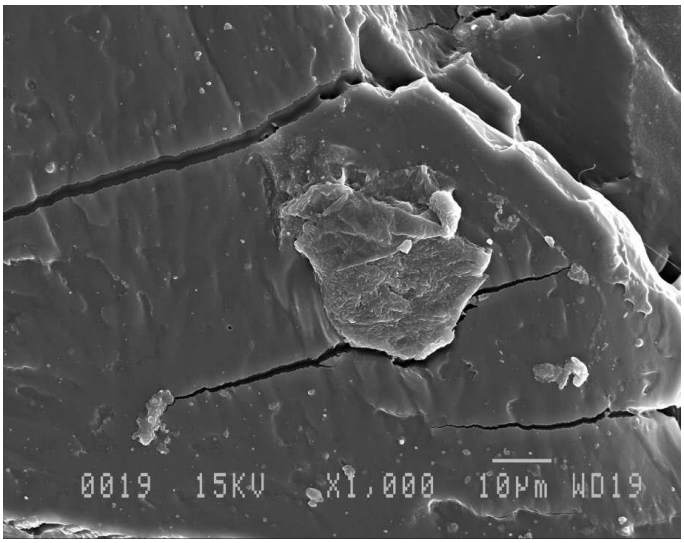

Figure 4 SEM images of PLA/SBRm (5%).

3.2 Density

The density of the raw rSBR and neat PLA (injection molded) are shown in Table 1. It can be seen that for rSBR, there is a slight density decrease with increasing particle size. Smaller rSBR particles might be more crosslinked as they were produced by grinding and larger particles break at their weakest point [14]. This explanation is confirmed by the low density of the unsieved materials which is close to the larger particle value. In the following sections, the neat PLA will be noted as 0; i.e. 0% rSBR.

Table 1 Density (+/- 1 kg/m^3) of the rSBR and PLA used.

Material	Density (kg/m^3)
PLA	1256
SBR1	1292
SBR2	1282
SBR3	1252
SBRm	1257

The density of the PLA/rSBR blends are presented in Figure 5. Since there are only small differences between the density of each material reported in Table 1 (between 1250 and 1300 kg/m^3), no clear tendency can be observed. But in most cases, the blends have densities lower than their components, a clear indication that some defects/voids are present in the molded samples as reported in Figures 1-4. There is also the possibility that the melt processing steps (extrusion and injection) slightly modified the densities of each material related to some degradation associated to the high temperatures used (rSBR volatiles/additives release). In general, the density slightly decreases with increasing rSBR content due to a larger amount of interfacial area created leading to more matrix-particle defects.

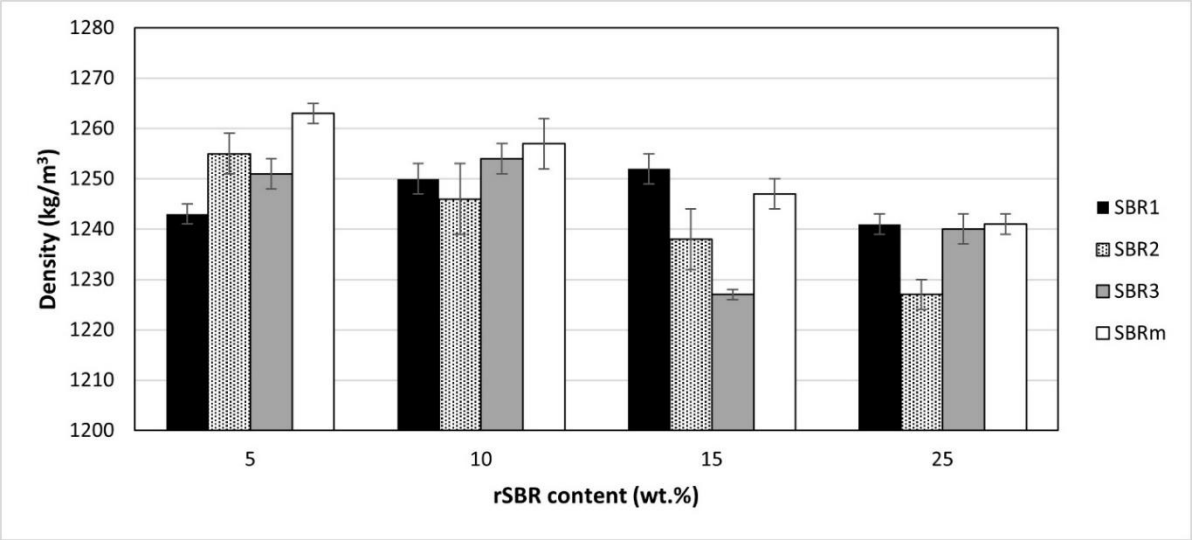

Figure 5 Density of PLA/rSBR blends (error bars represent one standard deviation).

3.3 Mechanical Properties

3.3.1 Tensile

As presented in Figure 6, the neat PLA showed the highest tensile strength (57.8 MPa) compared to the PLA/rSBR blends in all formulations. This is expected as not only the tensile strength of rSBR (around 4.2 MPa) is lower than that of PLA matrix [33], but rSBR particles (crosslinked) can act as stress concentration point at the interface of binary blends facilitate crazing and interfacial debonding. Consequently, the tensile strength decreases with increasing rubber content. Similar results have been reported in the literature as adding a soft rubber phase decreases the tensile strength for tire rubber residues in polypropylene (PP) [34] and polyethylene [35].

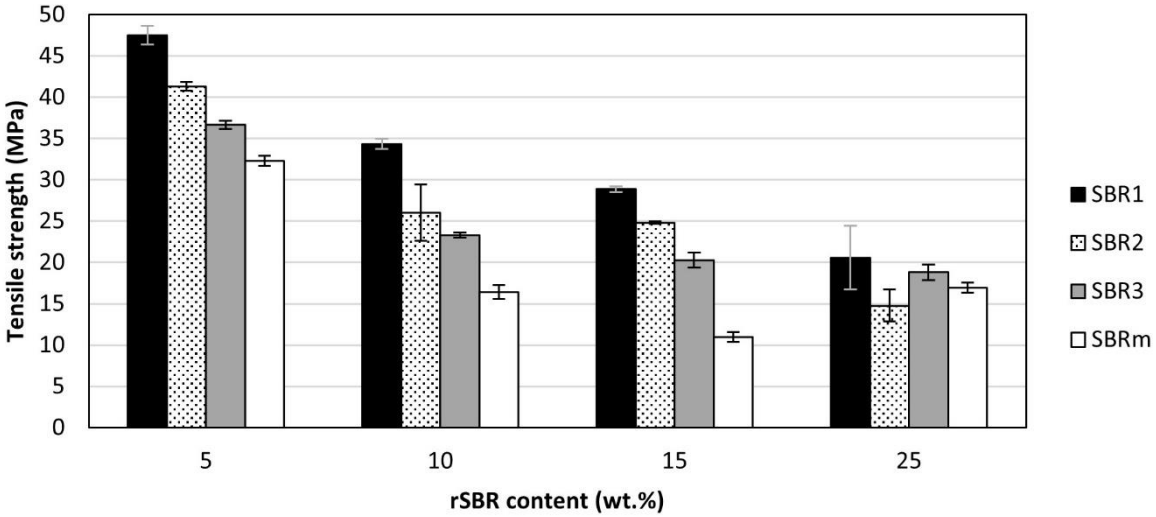

Figure 6 Tensile strength of the PLA/rSBR blends (error bars represent one standard deviation).

Nevertheless, up to 15% rSBR, there is a difference between the different rSBR particle sizes as SBR1 always produced higher tensile strength and SBRm showed the lowest. This difference between the particle sizes can be important as it varies between 21% and 163% at low SBR concentration (5-15 wt.%). Nevertheless, all samples gave similar results at 25% rSBR probably due to particle-particle interaction (contact) starting to become significant and possible agglomeration indicating a more significant role of blend compatibility and interface quality controlling the blends tensile strength at high filler content. There is reports in the literature that composites tensile strength depends on the particle size, interfacial adhesion and particle content [36]. As predicted by several models, both particle size and loading increases had a negative effect on tensile strength [36].

But different tensile strength values are an indication of different surface properties of the particles and/or different interfacial conditions. It has been shown in previous studies that mechanical forces during the recycling process can partially break the crosslinked structure of rSBR (partial regeneration) [10]. However, this phenomenon is limited to the particles' surface (thin region), leaving the core's (internal part) morphology unchanged [14]. Thus, rSBR particles might have lower mechanical strength for their skin (exterior = less crosslinked) compared to their core (interior = more crosslinked). Since smaller rSBR particles (SBR1) have a higher specific surface area, it is expected that they will display better tensile properties leading to better interfacial interaction between the particles and the thermoplastic molecules generating less structural defects. It is also likely that PLA has a better interfacial adhesion with smaller recycled rSBR particles. On the other hand, lower tensile properties for larger particles (SBR2, SBR3 and SBRm) can be related to particle agglomeration and dispersion problems resulting in stress concentration points and weak interfacial adhesion limiting stress transfer and premature failure in agreement with similar reports [37].

Figure 7 shows that the tensile modulus determined through the stress-strain curves slightly decreases with increasing rSBR content compared to neat PLA (1.1 GPa). This is again expected since the modulus of rSBR (around 0.31 GPa) is lower than the matrix inducing lower rigidity [38]. But, contrary to the tensile strength in Figure 6, the effect of particle size is not significant here indicating that all the particles had similar effect on tensile modulus.

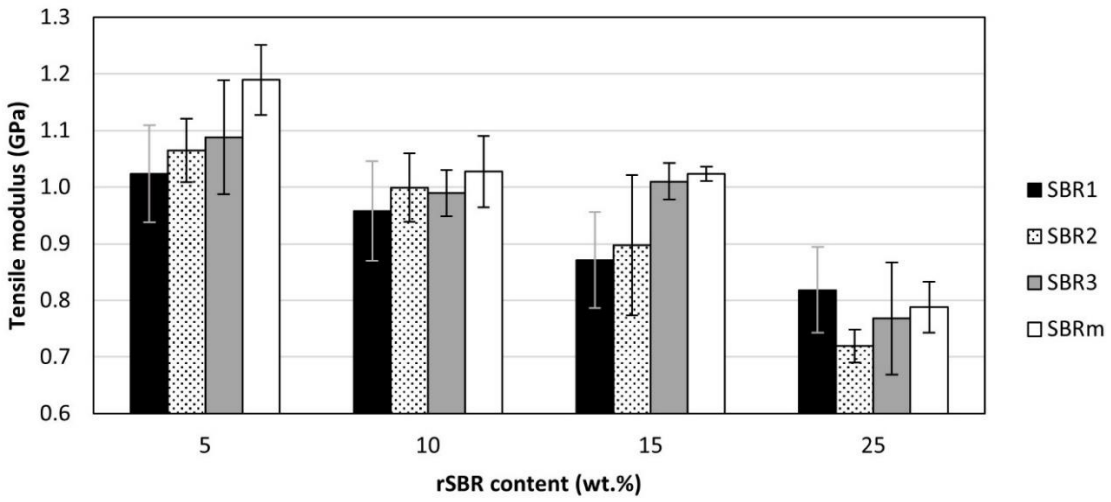

Figure 7 Tensile modulus of the PLA/rSBR blends (error bars represent one standard deviation).

The neat PLA showed the highest elongation at break (12%). As presented in Figure 8, the presence of rSBR decreased the value for the blends due to the crosslink nature of the rSBR particles without enough freedom to entangle with the matrix molecules to create strong interfacial bonding. But up to 15%, there is no significant difference between the different rSBR contents. The trends are also very similar to tensile strength as smaller particles produced higher values, but no significant differences are observed at higher rSBR content (25%).

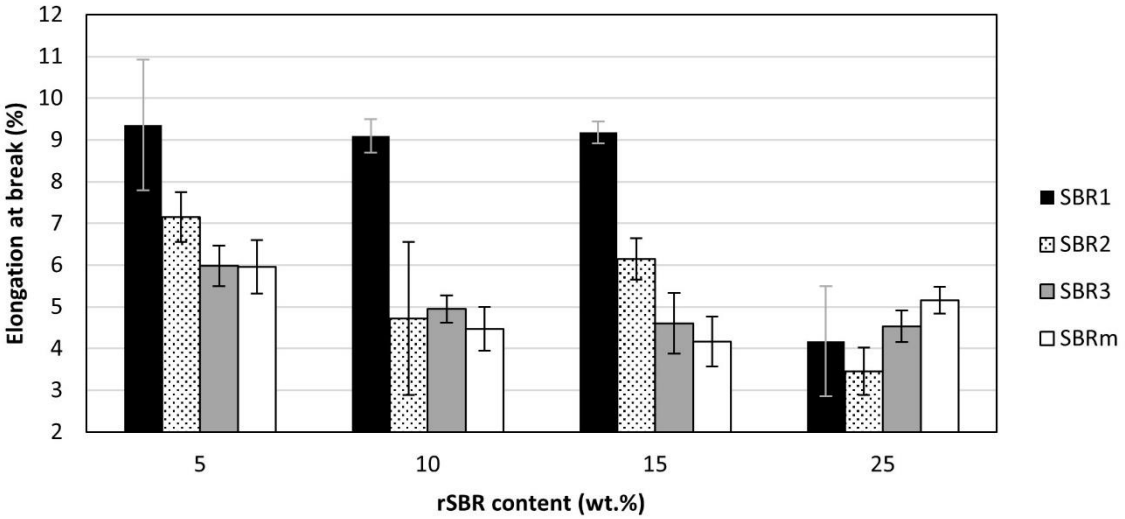

Figure 8 Elongation at break of the PLA/rSBR blends (error bars represent one standard deviation).

The literature shows that tensile failure in polymers is related to the average distance and diameter of microcracks [38]. Under stress, the interface between the polymer and the rubber should be the first to break, resulting in a microcrack with roughly the same diameter as the particle. Blends with SBR1 most likely initiated the smallest failures, since they had the smallest particles. Furthermore, these blends probably had a higher average distance between microcracks, since SBR1 had seemingly the most uniform distribution in the matrix (Figure 1). Thus, blends with SBR1 probably had the highest average distance and lowest diameter of microcracks, explaining their relatively higher elongation at break. But at 25% rSBR, the weak links between rSBR particles are probably too numerous (particle-particle contact and agglomeration), explaining the elongation at break drop and the similar values for different particle sizes. So, the more uniform is the particle distribution, the less chance of particle aggregation there is to avoid micro-cracks generation.

3.3.2 Flexion

The neat PLA had a flexural modulus of 3.27 GPa and Figure 9 presents the results for all the PLA/rSBR blends. As for the tensile modulus (Figure 7), the values are decreasing with increasing rSBR content (from 5 to 25% wt.), but there is no significant effect of particle size. This behavior might be related to the fact that in flexion, a combination of tensile and compression forces is present inside the sample, where both effects might cancel out and the interfacial state might not be as important as for other mechanical properties taking into account the intrinsic properties of the particles themselves (low modulus rubber compared to the matrix).

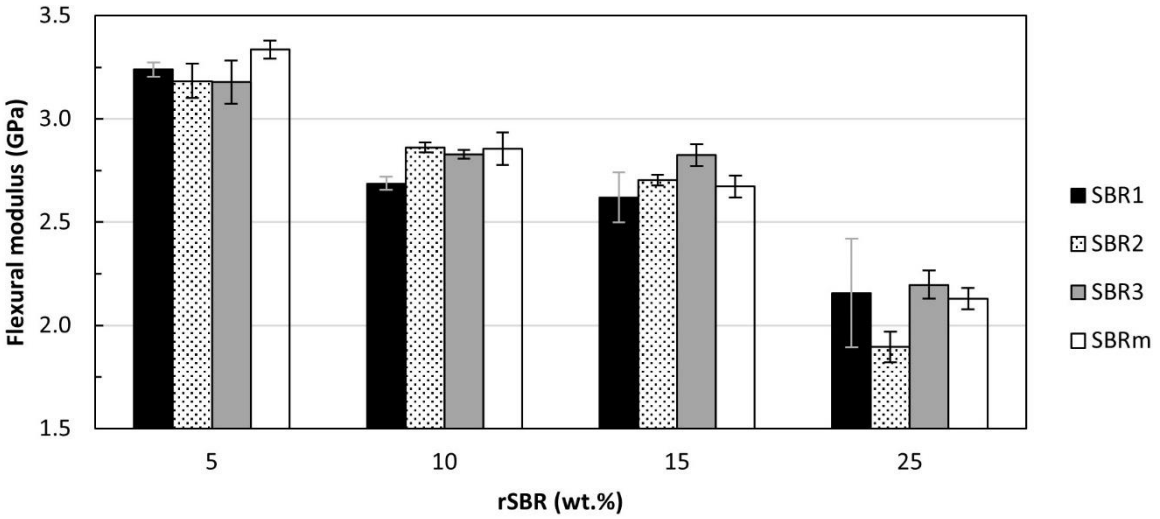

Figure 9 Flexural modulus of the PLA/rSBR blends (error bars represent one standard deviation).

3.3.3 Impact

The neat PLA had an impact strength of 20 kJ/m^2 and the results for all the compounds are presented in Figure 10. As for the other mechanical properties (tension and flexion), the value slowly decreases with increasing rSBR content. This might again be related to limited interfacial adhesion between both phases as limited energy was transferred to the rubber particles to absorb and the particles act as stress concentration points (crack initiation) as seen in Figure 4. However, a study by Rios-Soberanis et al. [39] on laminated PLA/rSBR blends mixed by an internal mixer showed that the impact strength initially decreased by 60% (up to 10 wt.% rSBR) compared with PLA, but the values eventually increased at higher rSBR concentration (60% wt.). It is possible that high enough rSBR content (not reached here because of processing problem due to the high viscosity of the compounds as particle content increases viscosity limiting possible injection molding), combined with the particle treatment Rios-Soberanis et al. [39] imposed on their material (pyrolysis and thermal shock) was enough to get better energy absorption. Comparatively, the addition of 10% wt. rSBR only led to a 45% decrease in PLA impact strength (from 20 to 11 kJ/m^2) indicating that the processing methods used (extrusion + injection) led to more adequate PLA/rSBR interfacial interactions retarding fracture phenomena. Previous work established that the extrusion feeding sequence (feeding the rubber phase in zone 1 and the matrix in zone 4) causes a direct transfer of shearing forces on the filler in the first part of the extruder, leading to smaller particle sizes and a narrower size distribution [13]. Partial regeneration of the rubber phase can also occur during extrusion, through a thermo-mechanical process, lowering crosslink density [10]. This allows improved chain mobility, enabling stronger interactions between the rubber phase and the matrix [13]. However, crosslink density reduction is favored with increasing particle size; i.e. larger surface area available to treat [14]. Since toughness increases with improved rubber/matrix adhesion and decreases with increasing rubber particle size, partial regeneration (breakdown of crosslinked network) during extrusion process (favored by particle size increase), might slightly offset the negative effects of increased particle size [13, 14]. Furthermore, smaller particle size can be

produced due to the processing conditions (particle break-up) which is expected to be more important with increasing particle size as larger particles are easier to break due to higher shear and elongation stresses [13]. This might explain why the blends with different rSBR sizes had similar impact properties. Additionally, during the melt processing, particle break-up is more likely to occur at their weakest point (lower crosslink density), leading to a higher number of stronger (higher relative crosslink densities) particles as reported by Macsiniuc et al. [14].

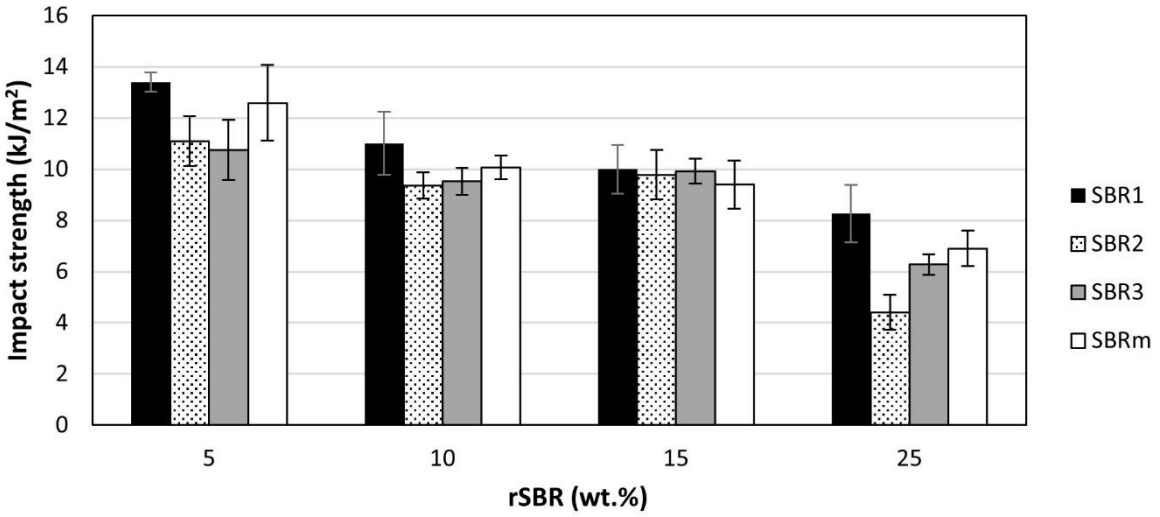

Figure 10 Impact strength of the PLA/rSBR blends (error bars represent one standard deviation).

It is known that the rSBR regeneration process in an internal mixer is influenced by all processing parameters (time, temperature and rotor speed), so it is expected that the same principles might also apply for the regeneration process in extrusion, and these parameters might be optimized for higher crosslink density and particle size reduction [14, 40]. Nevertheless, further studies are needed to understand the complex relations between rubber regeneration (crosslink density), particle size distribution (including break-up) and processing conditions.

3.4 Hardness

The neat PLA has a Shore D hardness of 84.6 and Figure 11 presents the result for all the PLA/rSBR blends. It can be seen that within experimental uncertainty, there is no significant effect of rSBR particle size on hardness variation, while the values are slightly decreasing with increasing rSBR content (from 5 to 25% wt.) which is attributed to the soft nature of rubber particles with low rigidity [41]. It can be concluded that the matrix is still controlling the surface properties of the compounds (good particle inclusion in PLA) at least for the range of conditions tested. Testing using the Shore A scale was also done, but no significant differences were observed between the samples.

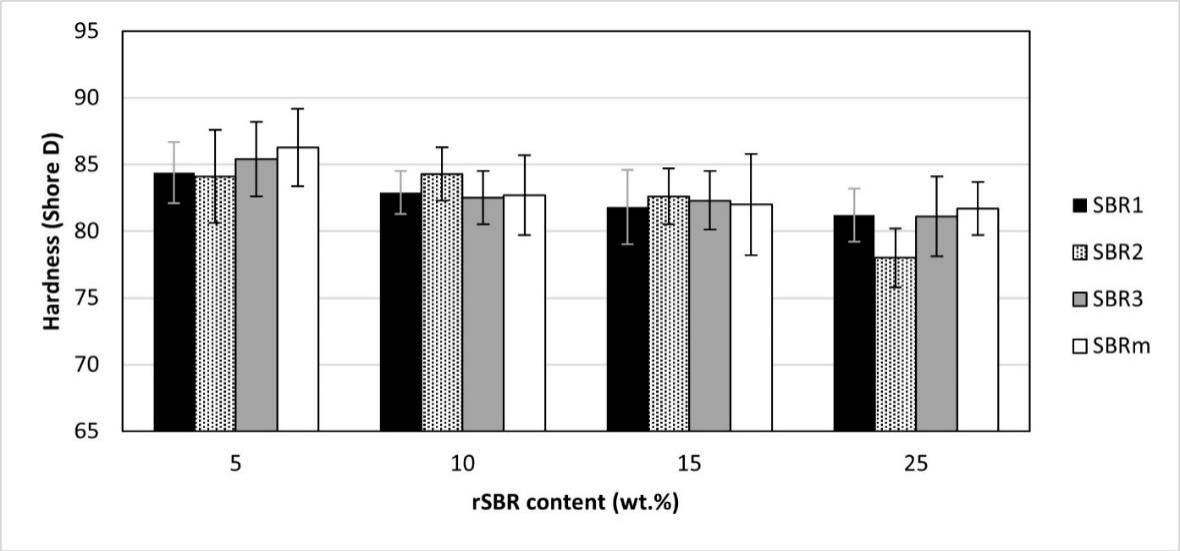

Figure 11 Hardness of the PLA/rSBR blends (error bars represent one standard deviation).

3.5 Fatigue

In order to get more information on the mechanical behavior of the blends, fatigue tests were carried out. To limit the experimental time and due to limited amount of materials, only the PLA/SBR1 blends with different SBR1 contents were analyzed as this information is seldom reported in the literature.

As a first step, the standard *S-N* curves are plotted in Figure 12 which represent the maximum stress applied on the material (*S*) as a function of the number of cycles to failure *Nf*. The plots show how the sample lifetime is affected by the stress level. In all cases, the neat matrix (PLA) performs better than the blends as *Nf* decreases with increasing rSBR content as for the other mechanical properties. Nevertheless, there is a limited difference between 0 and 5% wt. indicating that the effect of particle addition is limited at low rSBR content (up to 5% wt.). As shown in Figure 4, as long as the number of particles is low, they are well mixed in the matrix and do not create high stress concentration points. But above a critical threshold (between 5% and 10%), the service lives significantly decrease. This indicates that at low rSBR content, the PLA matrix is controlling the fatigue resistance, while substantial decreases are observed at higher content because of particle-particle interaction occurs which seems to control the fatigue behavior. Finally, at even higher concentration (10% and above) another plateau is reached, and the fatigue life does not change significantly with increasing rSBR content.

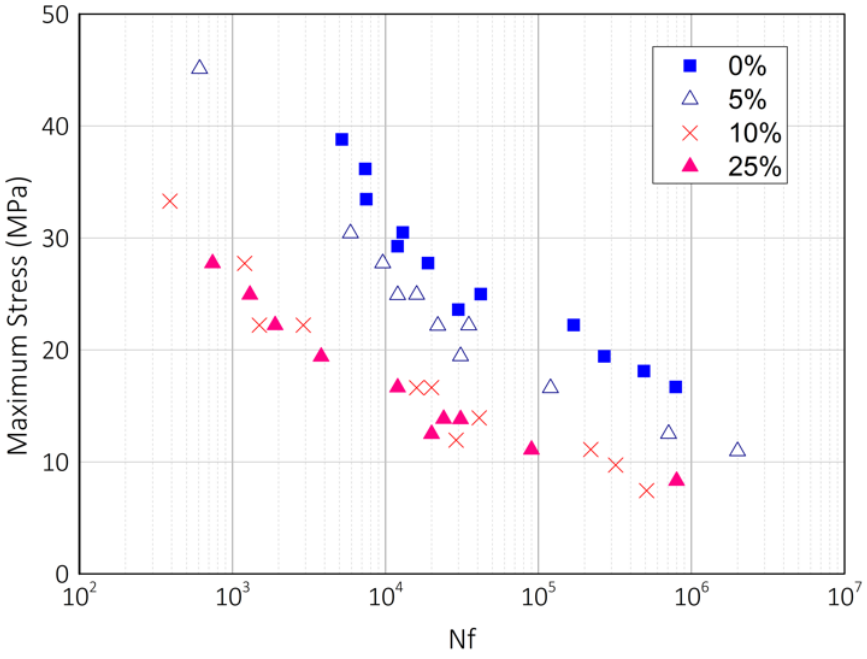

Figure 12 Fatigue behavior of PLA/SBR1 blends with different SBR1 contents.

The fatigue life difference observed between 5% and 10% rSBR is not obvious depending on which properties is analyzed. For example, tensile strength (Figure 6) exhibits a similar difference, while impact strength (Figure 10) and elongation at break (Figure 8) present no significant variation between these two ratios.

3.6 Instrumented Indentation

As a reminder, historical theoretical developments are limited to the mechanics of contact between a tip and a homogeneous/isotropic material. However, all materials are in fact composites at a given scale depending on the presence of different components such as grains, fillers or phases inside a matrix. Typical examples are cement-based materials [42], metals [43] or bones [44], which can be described as homogeneous materials at a macroscopic scale (cm or larger), but have to be treated as heterogeneous materials at finer scales. Heterogeneity can be a source of difficulties when assuming a continuous media. The latter implies a stress-strain relationship and thus a constant indentation hardness (H) whatever the scale of measurement [42]. For heterogeneous materials, variations in indentation curves and results are expected as the measurements will differ depending on the indentation locations with respect to the tip-material contact using a specific representative volume element (RVE). These non-uniformities are actually the origin of variation (lack of reproducibility) in the measurements. To avoid any microstructural effects and obtain homogenized properties (rather than separate responses from the different phases), a parameterization of the tests should be set with the objective of reaching an indentation depth h well above the size of any inclusions D (i.e. $h \gg D$: in general $h > 6D$ [45]).

Preliminary results showed that a typical depth h of about 7 to 8 µm is necessary (Figure 13) which is, when analyzing the surface and the dimensions of the rSBR (Figures 1, 2, 3 and 4), not in the theoretical value previously mentioned. This means that caution must be made when analyzing the results from instrumented indentation in our case.

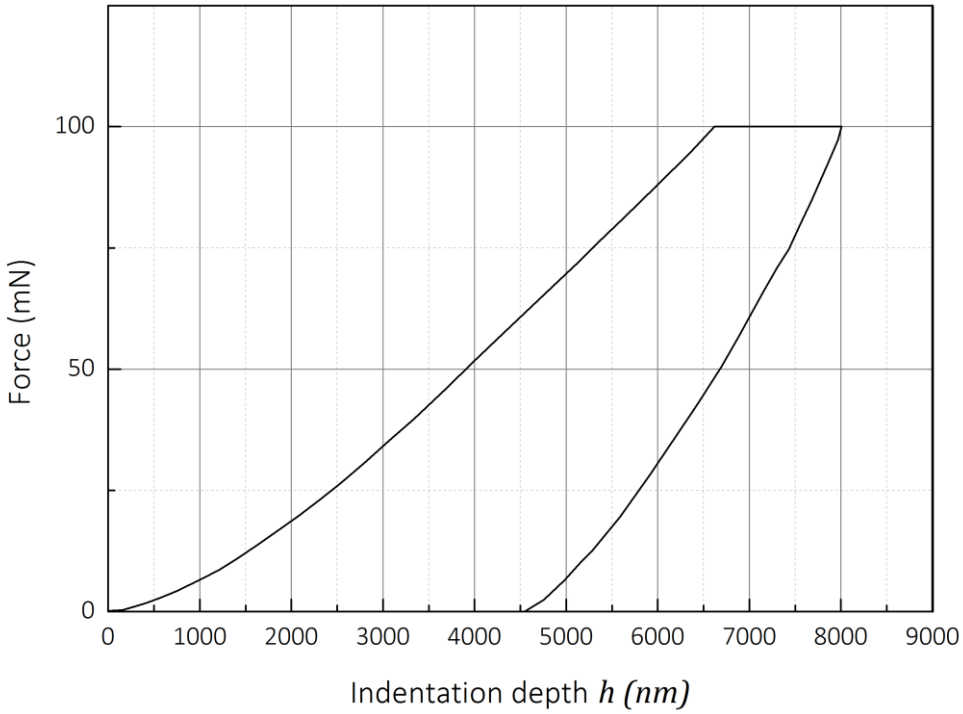

Figure 13 Load-depth curve for a 15% SBR1/PLA blend.

The protocol develop from previous works was carried out [21], including a holding time to dissipate viscous effects. Tests were carried out on SBR1/PLA blends (0% to 25% SBR1) by controlling the load until 100 mN with a holding time of 30 s (the loading and unloading rate are the same). Each sample was indented following a matrix of 9 indentations with 100 µm spacing between each indentation. A typical curve is presented in Figure 13.

The local modulus is then calculated from Hertz theory [46]. As this theory is based on the contact between two deformable solids, the combined modulus introduced which is generally called the reduced modulus (E_r), is defined as:

$$\frac{1}{E_r} = \frac{1-\nu_1^2}{E_1} + \frac{1-\nu_2^2}{E_2} \tag{7}$$

where E_1 and ν_1 are respectively the elastic modulus and Poisson ratio of the sample (here PLA/rSBR blends), while E_2 and ν_2 are the elastic modulus and Poisson ratio of the indentor (diamond tip). E_r is then calculated from the indentation curve and theoretical consideration (see section 2.3).

The reduced modulus (E_r) is often used because no assumption is needed to obtain local information (as it is the case for the local moduli including an assumption on the Poisson ratio).

The results of the PLA/SBR1 blends are promising because they show a low dispersion in the results with respect to the standard deviations obtained (Table 2). The results show a decrease in the local mechanical properties with increasing SBR1 content in the matrix. These results follow the same trends observed with the others macroscopic mechanicals properties except for the value at 25% SBR1 (very high modulus) which is difficult to explain. One possibility may be related to the very localized measurement technique; i.e. the indentation area investigated may have been in a part of the blend without rSBR (or a very low content).

Table 2 Indentation results for the samples tested.

Sample	E_r (GPa)	E (GPa)	Standard deviation (GPa)
Diamond (indenter)	-	1140	-
0% SBR1	1.98	1.73	0.03
5% SBR1	1.89	1.64	0.09
10% SBR1	1.85	1.59	0.13
15% SBR1	1.16	0.99	0.06
25% SBR1	2.31	1.95	0.16

Then, when looking at the global mechanical properties (Figure 14), differences can be observed between the local modulus and the modulus obtained from the macroscopic tensile test which is an observation commonly found in the literature [47]. This phenomenon is known as indentation size effect (ISE) which was reported for several polymers [48, 49]. The ISE is related, not only to a poor estimation of the projected area of contact due to a blunt tip, but also to surface roughness and energy dissipated at the surface. Nevertheless, the trends are similar up to 15%. So the local property seems to present a good trend up to 15%, but cautions must be made as these are only preliminary results.

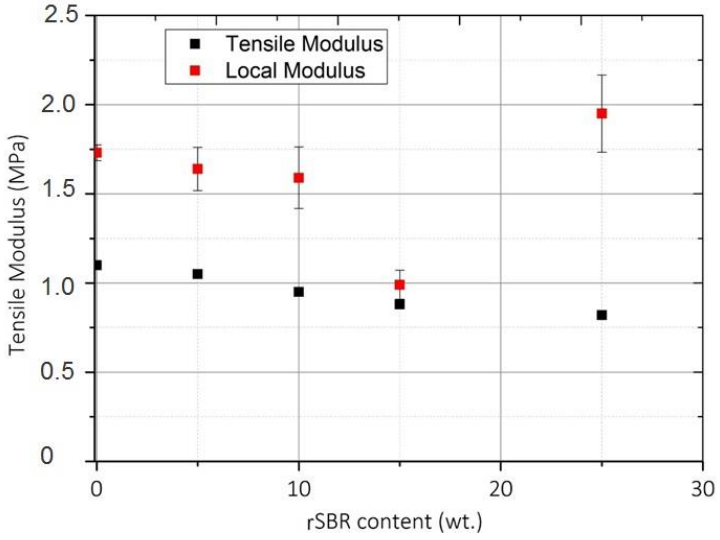

Figure 14 Comparison between the local and global modulus (error bars represent one standard deviation).

4. Conclusion

The structure and properties of poly(lactic) acid (PLA) and recycled styrene butadiene rubber (rSBR) from waste rubber powder blends mixed by extrusion and molded by injection were studied. The samples were prepared to study the effect of rSBR content (0 to 25% wt.) and particle size (125 to 1000 µm). From the samples produced, a complete set of characterization was performed including morphology, density, tensile and flexural properties, impact strength, and hardness as well as fatigue and indentation.

The results showed that limited differences were observed for the density since all the particles had similar values (between 1250 and 1300 kg/m^3). Only slight variations were observed due to some interfacial defects related to the rSBR particle sizes and interfacial interaction. Similarly, limited variation in Shore hardness (A and D scale) were observed because the rSBR particles were well embedded and this surface property was controlled by the matrix (PLA) in this case.

For the mechanical properties, all the values decreased with increasing rSBR content due the rubbery (elastic) nature of the dispersed phase and the limited interfacial interactions (confirmed by SEM). The same trends were observed in the case of fatigue resistance and instrumented indentation with, respectively, a threshold around 15%. These initial results tend to provide evidence of the interest in using a combination of fatigue and nanoindentation techniques to characterize two-phase materials. Nevertheless, some issues still need to be addressed to improve the measurements made, especially for instrumented indentation.

Finally, these results represent a first step towards the development of sustainable materials based on recycled rubber embedded inside a biosourced matrix. Nevertheless, more work is needed to improve on these results and produce resins for different applications like packaging, material handling, transportation, etc. This can be done by interfacial compatibilization via rSRB surface treatment (chemical, physical and thermal) and/or coupling agent addition to decrease particle agglomeration and improve interfacial adhesion.

Acknowledgments

The authors would like to thank the financial support of the Natural Sciences and Engineering Research Council of Canada (NSERC) and the Research center for high performance polymer and composite systems (CREPEC), as well as the Centre de Recherche les Matériaux Avancés (CERMA) and the Centre d'Étude et de Recherche sur les Élastomères (CERMEL) for technical and financial support. The technical help of Mr. Yann Giroux and Mr. Mathieu Venin was also highly appreciated.

Author Contributions

Conceptualization, D.R. and F.L.; methodology, D.R.; validation, D.R. and F.L.; formal analysis, E.C., J.C.M. and M.M..; investigation, E.C., J.C.M. and M.M.; resources, D.R. and F.L.; data curation, D.R. and F.L; writing—original draft preparation, E.C., J.C.M. and M.M.; writing—review and editing, D.R., A.F. and F.L.; visualization, D.R.; supervision, D.R. and F.L.; project administration, D.R. and F.L.; funding acquisition, D.R. All authors have read and agreed to the published version of the manuscript.

Funding

This research was funded by NSERC, grant number RGPIN-2016-058958.

Competing Interests

The authors have declared that no competing interests exist.

References

1. Williams SE, Davis SC, Boundy RG. Transportation energy data book: Edition 35. Oak Ridge: Oak Ridge National Lab.; 2017.
2. Veilleux J, Rodrigue D. Properties of recycled PS/SBR blends: Effect of SBR pretreatment. Prog Rubber Plast Recycl Technol. 2016; 32: 111-128.
3. Adhikari B, De D, Maiti S. Reclamation and recycling of waste rubber. Prog Polym Sci. 2000; 25: 909-948.
4. Fazli A, Rodrigue D. Recycling waste tires into ground tire rubber (GTR)/rubber compounds: A review. J Compos Sci. 2020; 4: 103.
5. Fazli A, Rodrigue D. Waste rubber recycling: A review on the evolution and properties of thermoplastic elastomers. Materials. 2020; 13: 782.
6. Michałowska M. The art of (up) recycling: How plastic debris has become a matter of art? Adv Environ Eng Res. 2021; 2. Doi: 10.21926/aeer.2104025.
7. Drumright RE, Gruber PR, Henton DE. Polylactic acid technology. Adv Mater. 2000; 12: 1841-1846.
8. Zhao Q, Ding Y, Yang B, Ning N, Fu Q. Highly efficient toughening effect of ultrafine full-vulcanized powdered rubber on poly (lactic acid) (PLA). Polym Test. 2013; 32: 299-305.
9. Mohammad N, Arsad A, Rahmat A, Sani NA, Mohsin MA. Influence of compatibilizer on the structure properties of polylactic acid/natural rubber blends. Polym Sci Ser A. 2016; 58: 177-185.
10. Yang JN, Nie SB, Ding GX, Wang ZF, Gao JS, Zhu JB. Mechanical properties, morphologies and thermal decomposition kinetics of poly (lactic acid) toughened by waste rubber powder. Int Polym Process. 2015; 30: 467-475.
11. Jo MY, Ryu YJ, Ko JH, Yoon JS. Effects of compatibilizers on the mechanical properties of ABS/PLA composites. J Appl Polym Sci. 2012; 125: E231-E238.
12. Yang J, Nie S, Zhu J. A comparative study on different rubbery modifiers: Effect on morphologies, mechanical, and thermal properties of PLA blends. J Appl Polym Sci. 2016; 133. Doi: 10.1002/app.43340.
13. Mahallati P, Rodrigue D. Effect of feeding strategy on the properties of PP/recycled EPDM blends. Int Polym Proc. 2015; 30: 276-283.
14. Macsiniuc A, Rochette A, Rodrigue D. Effect of SBR rubber particle size distribution on its thermo-mechano-chemical regeneration. Prog Rubber Plast Recycl. 2013; 29: 217-238.
15. Poisson JL, Lacroix F, Meo S, Berton G, Ranganathan N. Biaxial fatigue behavior of a polychloroprene rubber. Int J Fatigue. 2011; 33: 1151-1157.
16. Cruanes C, Deffarges MP, Lacroix F, Méo S. Modeling of the thermomechanical behavior of rubbers during fatigue tests from infrared measurements. Int J Fatigue. 2019; 126: 231-240.
17. Harbour RJ, Fatemi A, Mars WV. Fatigue life analysis and predictions for NR and SBR under variable amplitude and multiaxial loading conditions. Int J Fatigue. 2008; 30: 1231-1247.
18. Ayoub G, Naït-Abdelaziz M, Zaïri F. Multiaxial fatigue life predictors for rubbers: Application of recent developments to a carbon-filled SBR. Int J Fatigue. 2014; 66: 168-176.
19. Ezeh O, Susmel L. On the notch fatigue strength of additively manufactured polylactide (PLA). Int J Fatigue. 2020; 136: 105583.

20. Ezeh O, Susmel L. Fatigue strength of additively manufactured polylactide (PLA): Effect of raster angle and non-zero mean stresses. Int J Fatigue. 2019; 126: 319-326.
21. Fradet C, Lacroix F, Berton G, Méo S, Le Bourhis E. Instrumented indentation of an elastomeric material, protocol and application to vulcanization gradient. Polym Test. 2020; 81: 106278.
22. Fradet C, Lacroix F, Berton G, Meo S, Le Bourhis E. Extraction of local mechanical properties of an elastomer by means of nanoindentation: Developpment of protocols and application. Mater Tech. 2017; 105: 1-7.
23. ASTM International. Standard test method for rubber property-durometer hardness. West Conshohocken: ASTM International; 2015; ASTM D2240.
24. ASTM International. Standard test method for tensile properties of plastics. West Conshohocken: ASTM International; 2014; ASTM D638.
25. ASTM International. Standard test methods for flexural properties of unreinforced and reinforced plastics and electrical insulating materials. West Conshohocken: ASTM International; 2010; ASTM D790.
26. ASTM International. Standard test methods for determining the izod pendulum impact resistance of plastics. West Conshohocken: ASTM International; 2010; ASTM D256.
27. Samuels L, Mulhearn T. An experimental investigation of the deformed zone associated with indentation hardness impressions. J Mech Phys Solids. 1957; 5: 125-134.
28. Oliver WC, Pharr GM. Measurement of hardness and elastic modulus by instrumented indentation: Advances in understanding and refinements to methodology. J Mater Res. 2004; 19: 3-20.
29. Fischer-Cripps AC. Nanoindentation. 3rd ed. New York: Springer; 2011. pp.213-233.
30. King R. Elastic analysis of some punch problems for a layered medium. Int J Solids Struct. 1987; 23: 1657-1664.
31. Wu X, Bourbigot S, Li K, Zou Y. Co-pyrolysis characteristics and flammability of polylactic acid and acrylonitrile-butadiene-styrene plastic blend using TG, temperature-dependent FTIR, Py-GC/MS and cone calorimeter analyses. Fire Saf J. 2022; 128: 103543.
32. Liang H, Rodrigue D, Brisson J. Characterization of recycled styrene butadiene rubber ground tire rubber: C ombining X‐ray fluorescence, differential scanning calorimetry, and dynamical thermal analysis for quality control. J Appl Polym Sci. 2015; 132. Doi: 10.1002/app.42692.
33. Lee SH, Hwang SH, Kontopoulou M, Sridhar V, Zhang ZX, Xu D, et al. The effect of physical treatments of waste rubber powder on the mechanical properties of the revulcanizate. J Appl Polym Sci. 2009; 112: 3048-3056.
34. Kakroodi AR, Rodrigue D. Impact modification of polypropylene-based composites using surface-coated waste rubber crumbs. Polym Compos. 2014; 35: 2280-2289.
35. Shaker R, Rodrigue D. Rotomolding of thermoplastic elastomers based on low-density polyethylene and recycled natural rubber. Appl Sci. 2019; 9: 5430.
36. Fu SY, Feng XQ, Lauke B, Mai YW. Effects of particle size, particle/matrix interface adhesion and particle loading on mechanical properties of particulate–polymer composites. Compos B Eng. 2008; 39: 933-961.
37. Fazli A, Rodrigue D. Effect of ground tire rubber (GTR) particle size and content on the morphological and mechanical properties of recycled high-density polyethylene (rHDPE)/GTR blends. Recycling. 2021; 6: 44.

38. Liao Y, Wells V. Estimation of complex Young's modulus of non-stiff materials using a modified Oberst beam technique. J Sound Vib. 2008; 316: 87-100.
39. Rios-Soberanis CR, Wakayama S, Sakai T, Rodriguez-Laviada JD, Pérez-Pacheco E. Manufacture of partially biodegradable composite materials based on PLA-tires powder: Process and characterization. Int J Polym Sci. 2013; 2013: 514951.
40. Macsiniuc A, Rochette A, Brisson J. State-of-the-art of thermomechano-chemical rubber regeneration. In: Recycled polymers: Chemistry and processing. Shawbury: Smithers Rapra Technology; 2015. pp.1-28.
41. Fazli A, Rodrigue D. Phase morphology, mechanical, and thermal properties of fiber-reinforced thermoplastic elastomer: Effects of blend composition and compatibilization. J Reinf Plast Compos. 2021; 0: 07316844211051749.
42. Constantinides G, Chandran KR, Ulm FJ, Van Vliet KJ. Grid indentation analysis of composite microstructure and mechanics: Principles and validation. Mater Sci Eng A. 2006; 430: 189-202.
43. Nohava J, Hausild P, Randall NX, Favaro G. Grid nanoindentation on multiphase materials for mapping the mechanical properties of complex microstructures. Proceedings of the IMEKO 2012 TC3, TC5 and TC22 Conferences, Metrology in Modern Context; 2010 November 22th-25th; Pattaya, Chonburi, Thailand. Berlin: ResearchGate.
44. Ulm FJ, Vandamme M, Bobko C, Alberto Ortega J, Tai K, Ortiz C. Statistical indentation techniques for hydrated nanocomposites: Concrete, bone, and shale. J Am Ceram Soc. 2007; 90: 2677-2692.
45. Constantinides G, Ulm FJ. The nanogranular nature of C–S–H. J Mech Phys Solids. 2007; 55: 64-90.
46. Hertz H. On the contact of elastic solids. Z Reine Angew Mathematik. 1881; 92: 156-171.
47. Wrucke AJ, Han CS, Majumdar P. Indentation size effect of multiple orders of magnitude in polydimethylsiloxane. J Appl Polym Sci. 2013; 128: 258-264.
48. Han CS, Nikolov S. Indentation size effects in polymers and related rotation gradients. J Mater Res. 2007; 22: 1662-1672.
49. Alisafaei F, Han CS, Lakhera N. Characterization of indentation size effects in epoxy. Polym Test. 2014; 40: 70-78.